DEVELOPMENT OF TRANSITION METAL DOPED POLYCRYSTALLINE ZnO FOR SPINTRONICS APPLICATIONS

SYNOPSIS

Submitted for the partial fulfilment of the requirement for the degree of

DOCTOR OF PHILOSOPHY

IN

PHYSICS AND MATERIALS SCIENCE

BY

NEHA KONDAL

Enrolment Number: 146954

Under the supervision of

Dr. Sanjiv Kumar Tiwari

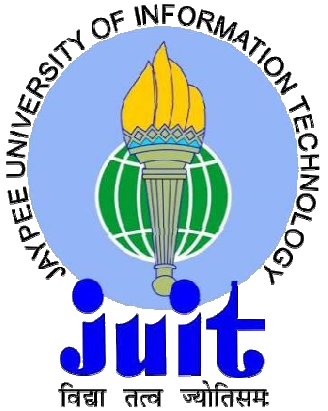

DEPARTMENT OF PHYSICS AND MATERIALS SCIENCE

JAYPEE UNIVERSITY OF INFORMATION TECHNOLOGY

WAKNAGHAT, DISTRICT SOLAN, H.P, INDIA

May 2018

Contents

1. Introduction.
2. Thermal and temporal evolution of microstructure and interface formation of grain by high temperature annealing.
3. Origin of polychromatic emission and defect distribution within annealed nanocrystalline ZnO and their effect on magnetic properties and spin-spin interaction.
4. Selectively enhanced different defect in nanocrystalline ZnO: A path to make p-type ZnO without doping by multistep annealing.
5. Development of CoO and NiO doped ZnO nanoparticles: A promising material for spin aligner.
6. Conclusion and future scope.

Introduction

In the field of microelectronics research, the available devices (based on numbers of transistors in unit area) are now rapidly approaching the limit of how small and closely packed these transistors can be implemented before the heat they generate cannot be dissipated fast enough, or unwanted quantum mechanical effects prevent them from functioning properly. Therefore, an alternative to conventional microelectronics is needed. This can be achieved by adding an extra degree of freedom, e.g. spins angular momentum orientation, to the flow of charge. Therefore, one of the goals is to build spin-based light emitting diodes that generate left or right circularly polarized light. In order to implement this idea the fundamental requirement is electron-spin injection, manipulation and detection in host semiconductor. Practically, spin manipulation is relatively straight forward, but injecting and detecting theses spin under practical condition is a challenging task because one need to find spin-polarized material (Spin aligner) in which most of the electron spins are aligned in a particular direction at room temperature e.g. room temperature ferromagnetism is essential. A promising material for this purpose could be transition metal doped ZnO based dilute magnetic semiconductors (DMS) , e.g. $Zn_xM_{1-x}O$ (M= Co, Ni, Mn) as spin aligner , and non-magnetic p- and n-type ZnO as base and recombinant material respectively. All of them being nano-structured, either by different preparation methods like chemical vapour deposition method (CVD), physical vapour deposition method (PVD), pulsed laser deposition method (PLD) , Sol-gel methods or modified/tailored defect structure. Keeping in view that the defect and spin densities also depend on spatial nature of nanostructures (quantum dots, nanowire, nanorods, and core-shell structure), a detailed characterization/analysis of their optical and magnetic properties, as well as their dependence on temperature and doping fraction, is mandatory before introducing any device. The advantage of choosing transition metal oxide over other oxides is that those magnetic ions will be incorporated iso-

electronically, thus providing localized magnetic moments without altering the crystal structure and carriers doping. Transition metal spins in undoped or n-type ZnO are usually coupled by large exchange energy and, at low doping concentration and low temperature, the sp-d exchange interaction leads to a large Lande g factor (more than twice as compared to free electron) which results in large Zeeman splitting of band edge related states.

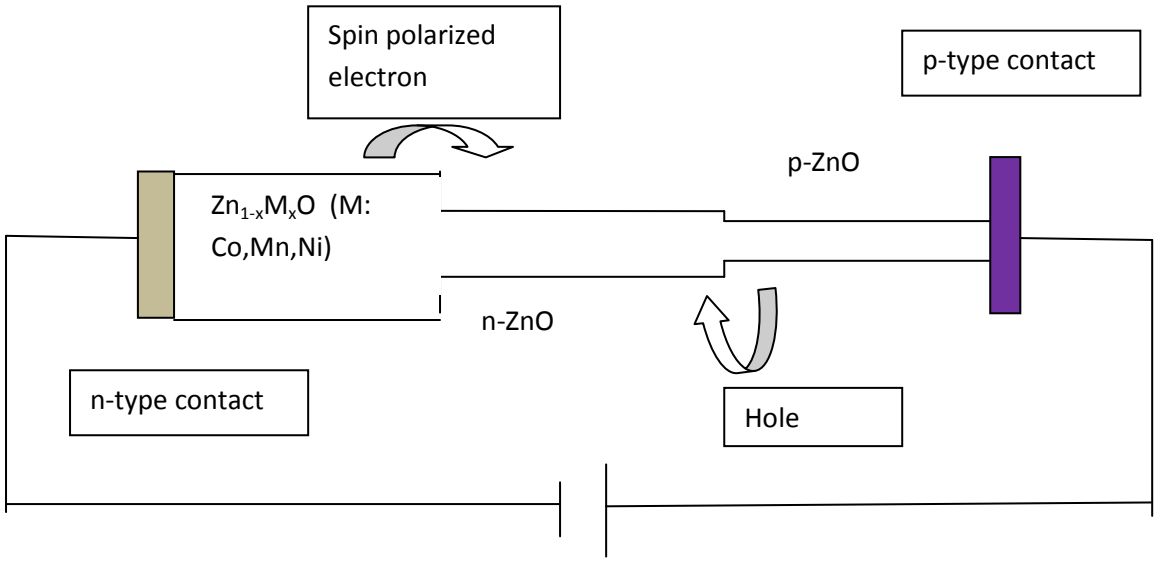

Figure 1: Proto type design of ZnO based spintronic device.

We exploit this enhanced Zeeman splitting to align the spins within the magnetic layer of ZnO. Subsequently, these spin-polarized electrons will be passed into the non-magnetic n-type ZnO. Depending on spin de-phasing times (which is of the order of nanosecond), the preferential spin orientation will survive up to a distance of 50-100 nanometre: therefore, by making a second ZnO nano-structured layer of thickness of about 100 nm, ZnO based spintronics device can be made. A prototype design of the this type of device is shown in figure 1. From scientific point of view, fundamentally this device should work as follows.

p-type ZnO (multi step sintered ZnO nanostructure or Cu doped) and n-type ZnO have almost same optical band gap , which makes it ideal for injection of hole from p type ZnO to

n type ZnO by proper electrical biasing. $Zn_xM_{1-x}O$ (M= Co, Ni, Mn) nanostructure are ferromagnetic in nature at room temperature. Hence it will act as source and suitable material for spin polarized electrons So far, only few spintronic devices have been made, which consists of quaternary II-VI magnetic semiconductors ($Be_xMn_yZn_{1-x-y}Se$) as spin aligner and p-type GaAs as host [1]. Use of quaternary magnetic semiconductor is restricted because of formation of magnetic phase; hence binary or tertiary magnetic material will be advantageous as spin aligner [2]. GaAs can be replaced by ZnO for this particular application because its band structure is the same in nature. As GaAs, ZnO conduction band (s-character) is twofold spin degenerated, whereas valence band (p-character) is fourfold degenerated. This degeneracy's are lifted in a magnetic field. Further, there are only two main reports which show injection and detection of spin polarized electrons. On one hand, R. Fiederling *et al*. Measure optical polarization of electroluminescence of GaAs based spintronic LED and, on the other hand, Y.Ohno *et al*. reported electrical spin injection in a ferromagnetic semiconductor hetero-structure [3, 4]. In ZnO based DMS, there is always a possibility of existence of secondary magnetic phase; recently Castro *et. al* has reported the formation of secondary magnetic phase of doped transition metal oxides which was barely detected in X-Ray diffraction spectra [5]. A. Savoyant and his co-workers had reported the interaction between magnetic ions by EPR hyperfine spectra at 5% Co-doping level [6]. Further, making of p-type ZnO is a very challenging task and till date there is no direct method to produce it.

The following fundamental problem of spin based deices leads to design our objective of thesis.

(a) Effect of spin-spin, and spin-lattice interaction at the interface of grains, and p-type and n-type ZnO has not been studied to the best of our knowledge.

(b) P-type ZnO means existence of excess zinc vacancies in sample, and interaction of these defects with Zn interstitial will result in donor-acceptor pair (DAP) formation.

The effect of DAP on magnetic properties has not been studied. Although, DAP signal has been reported in low temperature photoluminescence and core-shell type structure [7].

(c) Similar to point (a) and to the best of our knowledge, effect of interface of single crystalline CoO and NiO doped ZnO with polycrystalline ZnO has not been studied. This is because spin-orbit interaction strength in polycrystalline ZnO is ~20 meV which is almost same as L-S coupling strength of Co +2 ions.

(d) Electroluminescence measurement and spin Hall measurement on this proposed device can give possibility of future use of ZnO based DMS in spintronic devices. It will also open new window for making spin based FET and MOSFET for use in electronic industries.

Therefore objective of the thesis is designed by keeping in mind "MATERIAL REQUIRED FOR SPINTRONIC DEVICES AND RELATED PROBLEMS". This leads to four main objectives of the present work.

1. Thermal and temporal evolution of microstructure and interface formation of grain by high temperature annealing.
2. Origin of polychromatic emission and defect distribution within annealed nanocrystalline ZnO and their effect on magnetic properties and spin-spin interaction.
3. Selectively enhanced shallow and deep donor defect in nanocrystalline ZnO: A path to make p-type ZnO without doping by multistep annealing.
4. Development of CoO and NiO doped ZnO based DMS: A promising material for spin aligner.

Objective 1: Thermal and temporal evolution of microstructure and interface formation of grain by high temperature annealing.

Figure 2 shows the schematic of conventional annealing (CA) and multi step annealing (MSA). In CA, sample temperature was raised at heating rate of 100 ^{0}C/min at desired final temperature (200, 400, 600, 800, 1000, 1100 ^{0}C) and kept there for two hours. Whereas, in MSA sample temperature was raised in steps while keeping the heating rate constant. In first step grain evolution is termed as thermal evolution and during residual time at constant temperature is termed as temporal evolution respectively. During temporal evolution grain growth is governed by equation, $d-d_0=Kt^n$ where, d_0 is initial grain size, t is annealing timet , $K = K_0 \exp(-Q/RT)$, $1<n<2$, Q is the activation energy and T is the annealing temperature, R is the universal gas constant respectively. Whereas in thermal evolution process grain growth is given as $d=d_0 \exp(-Q/RT)$. In CA all parameters remains constant except t, whereas in MSA effective annealing time and Q changes at each steps. Thus process of CA and MSA will have different growth mechanism and defect distribution.

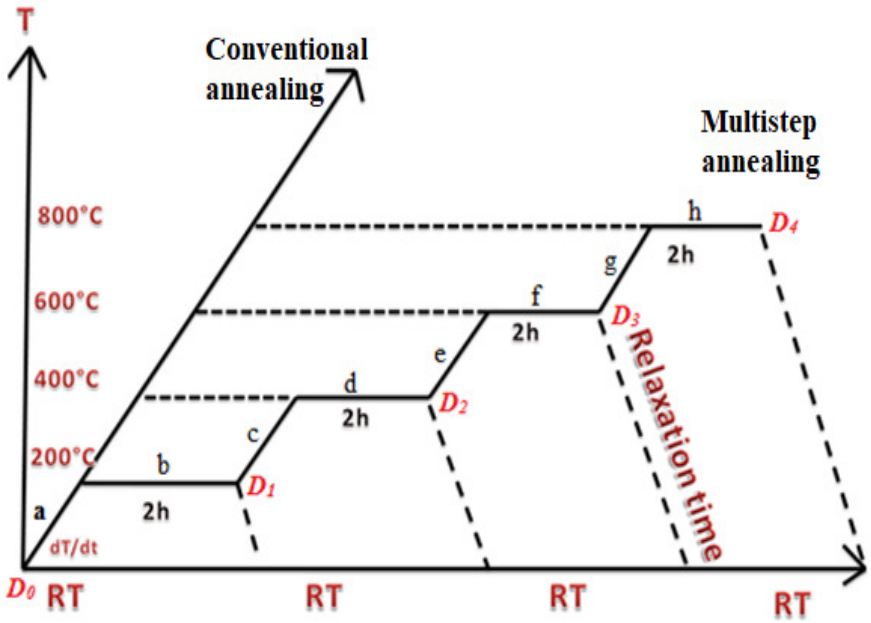

Figure 2. Schematic for conventional and multistep annealing

(a) Conventional annealing

XRD pattern of pristine and annealed sample (at temperature 200, 400, 600, 800, 1000 and 1100 ^{0}C) reveals polycrystalline nature. On annealing XRD peaks shifts towards higher angle till 800 ^{o}C then relax to lower diffraction angle for 1000^{o}C and 1100^{o}C annealed sample as shown in figure 3(a) and figure 3(b) respectively. The grain size increases from 67 nm (pristine) to 93 nm (at 800 ^{0}C), then decreases to 65 nm after annealing at 1100 ^{0}C. This is due to high concentration of Zn_i inside the lattice, which produces uniform stress with tensile component parallel to c-axis, relaxation towards lower angle indicates the lowering of oxygen vacancies (V_O) and hence shows a gradual transition from compressive stress to tensile stress. The change of Zn_i concentratio with annealing temperature can be demonstrated by examining peak intensity of [002] line in XRD data, figure 3(c). Grain growth and defect diffusion occurs up to 800 ^{O}C, further annealing at higher temperature improve densification. In the process of densification, grains break into smaller particles resulting in deviation of XRD peaks toward its original value followed by relaxation in stress. Variation of grain size with temperature were fitted with equation $d=d_0 \exp(-Q/RT)$, where Q, R, d and d_0 are activation energy barrier for diffusion mediated growth, universal gas constant, grain size at annealed temperature T and pre exponential factor respectively, fitting yields Q equivalent to 385 kJ/mol. The calculated activation energy (Q=385 kJ/mol) for grain growth at heating rate of 100 ^{O}C/min is close to the diffusion barrier of zinc and oxygen in polycrystalline ZnO [8]. Therefore, temperature mediated diffusion results into redistribution of defects. Zn_i diffuse towards surface of grain, whereas oxygen remains somewhere in interior of grain. During annealing in air, zinc diffusion is isotropic with respect to crystal direction/orientation, zinc possess activation energy of 131 kJ/mol and 116 kJ/mol for diffusion along a,b and c direction respectively [9] . Therefore, zinc has

equal probability to diffuse along all crystal direction. These results lead to the development of grain growth model based on diffusion of excess Zn_i. For modelling of diffusion mediated growth of the particle it was assumed that particles are spherical and chemical potential of excess Zn_i at surface differs from the value of the same in interior of the grain. Annealing induces diffusion of Zn_i (or Zn_i ion) from bulk to surface via reaction $Zn_{i,b}$-$Zn_{i,s}$ followed by oxidation reaction Zn_i+ ½ O_2= ZnO, where subscripts *s* and *b* refer to surface and bulk respectively. Diffusion equation for excess Zn_i in sphere of radius R given as, $\nabla^2 C = \frac{1}{D}\frac{\partial C}{\partial t}$, Where, *C* and *D* indicates concentration and diffusion coefficient of Zn_i respectively. We assume uniform radial diffusion of Zn_i and restrict our calculation to radial growth only. Hence, above equation can be modified as

$$\frac{\partial^2 C}{\partial r^2} + \frac{2}{r}\frac{\partial C}{\partial r} = \frac{1}{D}\frac{\partial C}{\partial t} \quad ,$$

The boundary conditions are $C(r,0)=C_0$ and $C(r,t)=C_s$. Where, C_0 and C_s represent bulk and surface concentration of Zn_i respectively. By taking into account the mass balance of Zn_i crossing the oxidized surface layer and assuming thickness (x) of new layer smaller than grain size ($x << R'$) , Where $x= R''^2-R'^2$, R'' corresponds to radius of newly formed layer. $\sigma = \rho_s (M_{Zn}/M_{ZnO})$, here, ρ_s, M_{Zn},and M_{ZnO} represent density of ZnO at surface, atomic weight of Zn and molecular weight of ZnO respectively. For the case of large annealing time ($t\rightarrow\infty$) and maximum oxidized layer thickness ($x\rightarrow x_m$) , slution of this equation is given as $-\ln\left[1-\left(\frac{x}{x_m}\right)^2\right]-\ln\frac{\pi^2}{8} = D\left(\frac{\pi}{R}\right)^2 t$,[10]. Hence annealed ZnO grain can be visualized as shown in figure 3(d), where, core of the particle represent bulk ZnO in this region there is no any diffusion of Zn_i or Zn ion, this region of particle is responsible for near band edge emission (NBE) which do not change with annealing temperature, surface modification or capping with polymer. Surface or shell of the annealed ZnO contains excess Zn_i which is

responsible for blue emission. Therefore, origin of visible emission in ZnO and their variation with annealing temperature is directly related to the different spetial region of particle. Spatial distribution of visible emission from annealed ZnO grains were confirmed by fluorescence imaging method using Nikon fluorescence microscope equipped with triple band excitation filter DAPI, FITC ,TRITC combined with appropriate set of dichromatic mirror [11].

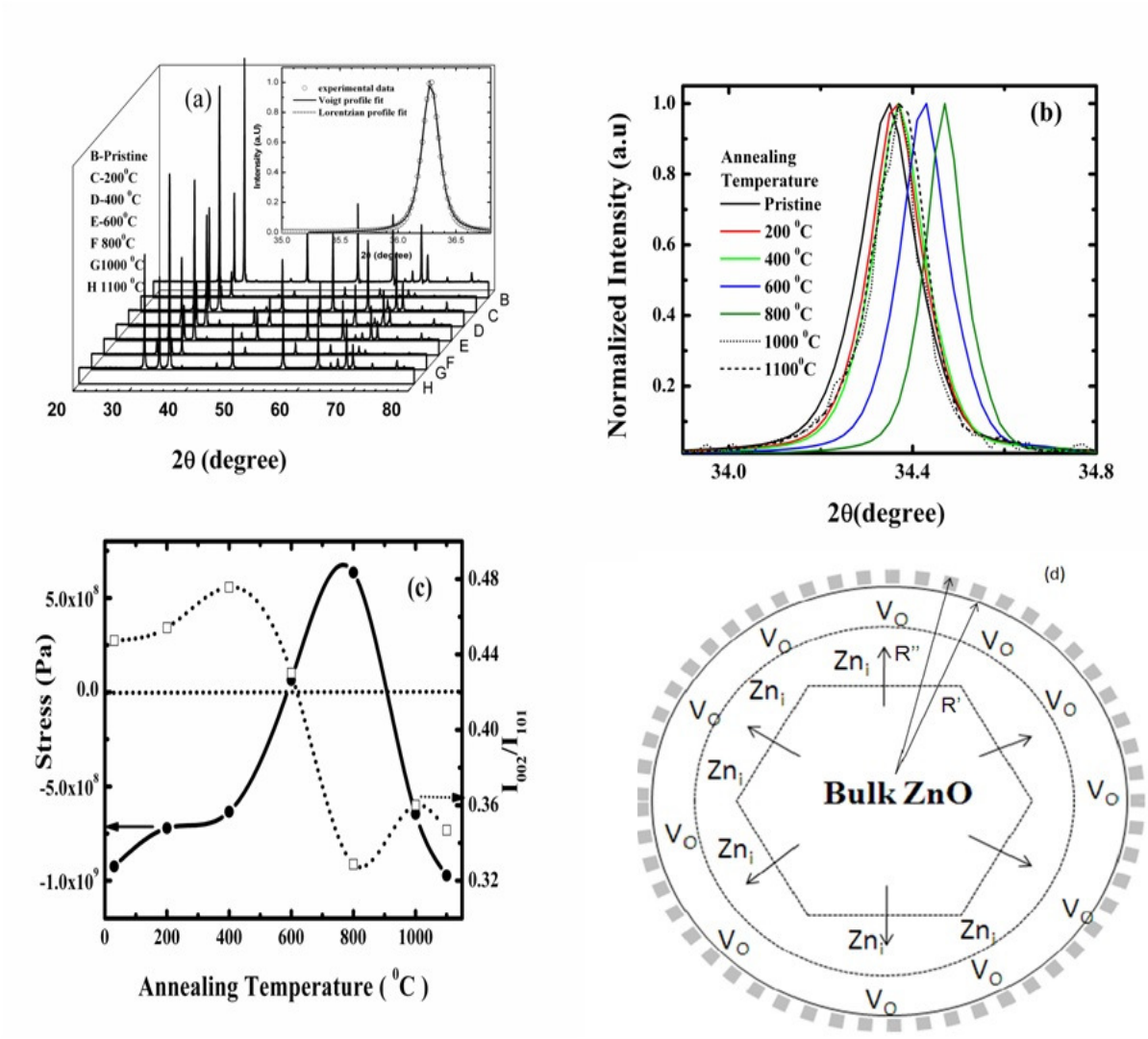

Figure 3. (a) XRD pattern of annealed samples, (b) variation of peak position at different annealing temperature, intensity is normalised to unity, (c) Variation of stress along c- axis and intensity ration with annealing temperature, (d) schematic representation of defect distribution within annealed grains.

(b) Multi step annealing (MSA)

In the first step of multistep annealing i.e. the step of thermal evolution, structural deformations, and defect evolutions are only temperature dependent. For thermal evolution theoretical model of grain growth suggests the exponential dependence of grain size on the annealing temperature as $d=d_0\ exp\ (\ -Q/RT)$, where d_0 is the initial grain size, Q is the activation energy and T is the annealing temperature, R is the universal gas constant. In step of temporal evolution of MSA, the defect evolution depended only on the residual annealing time e.g. $d-d_0=Kt^n$, where , K is rate constant and t is the annealing time respectively. Thermal growth is totally diffusive in nature and temporal growth follows the power law behaviour.

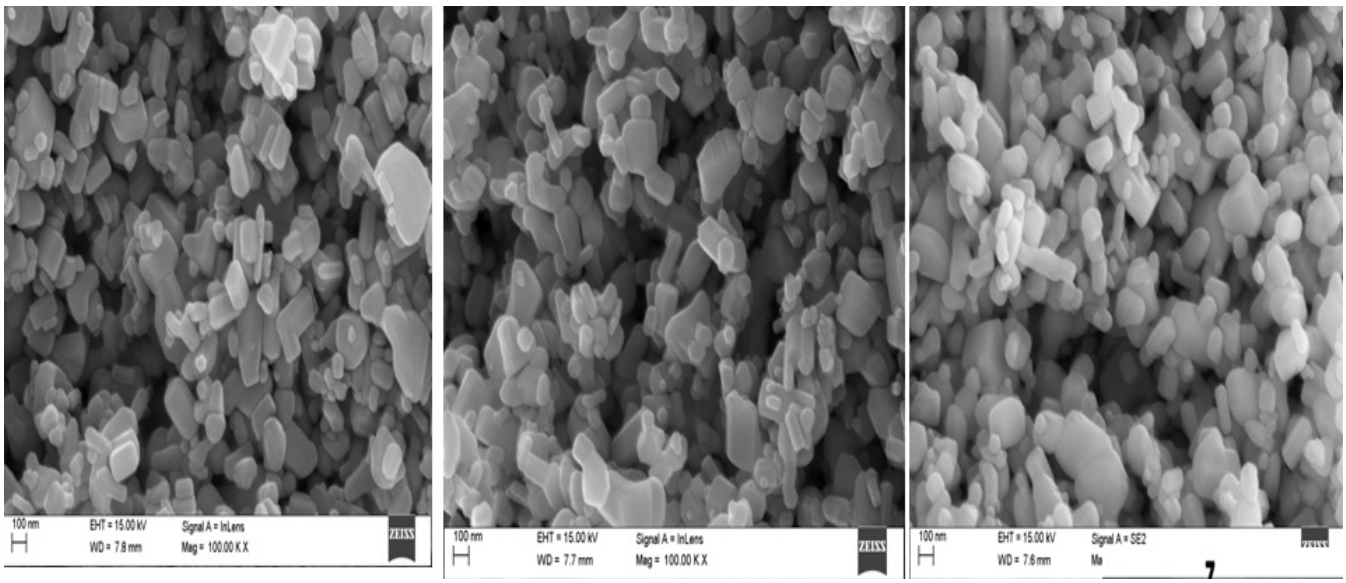

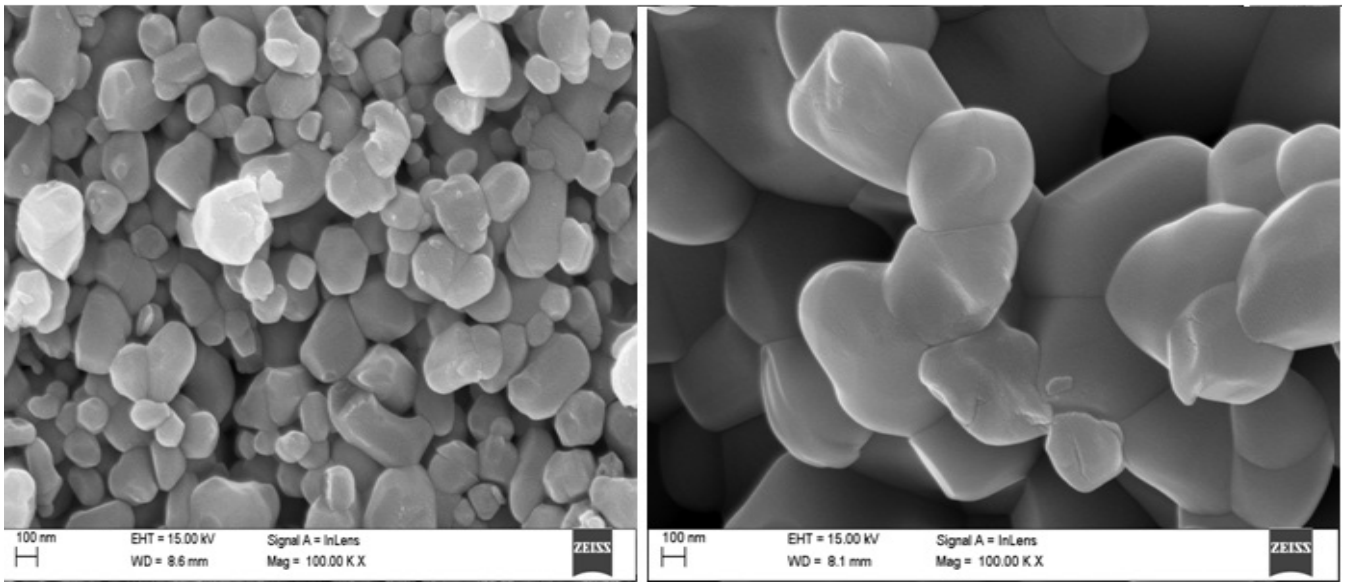

Above pictures shows the scanning electron microscope (SEM) image of pristine as well as MSA annealed samples at 100 nm resolutions. It reveals that most of the particles (> 75 %) are hexagonal/rod like structure (marked with line just below). Since, diffusion constant is temperature dependent hence grain growth and defect distribution for MSA process is modelled by solving diffusion equation in cylindrical co-ordinate system. From the SEM image grain evolution is assumed to take following steps.

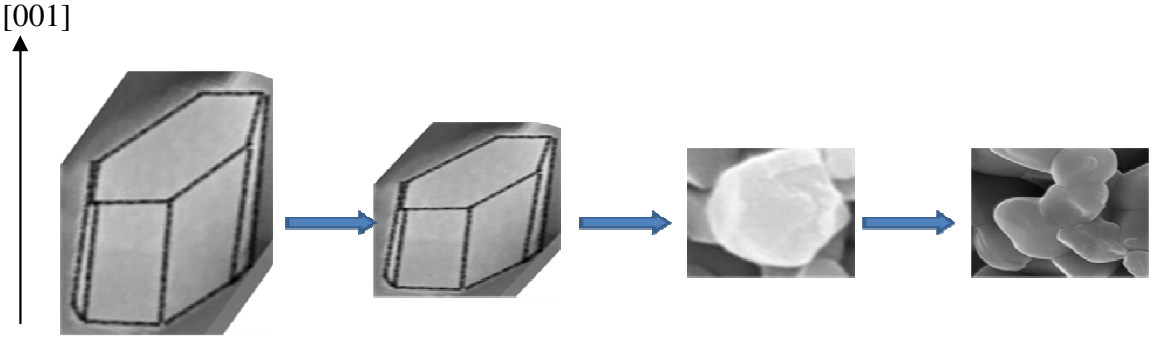

We calculated length and diameter of rod like structure and it was found that with increasing annealing temperature up to 600 ^{0}C aspect ratio (rod's length/diameter) decreases and morphology changed from regular shape to irregular shape as shown pictorially above, with further increase of temperature (till 800 ^{0}C) grain boundary formation start taking place. Therefore, it is very realistic to assume that in MSA process growth is also radial e.g. along a, b crystal direction and diffusion of defects along the curvature of surface give rise to formation of grain boundary. Therefore, grain growth and defect distribution in MSA process was modeled by solving diffusion equation, with effective diffusion constant and appropriate boundary condition in cylindrical co-ordinate system. Only radial growth is considered, whose solution consists Bessel function. Therefore it is expected that concentration of defects are distributed like Bessel function within grains, which is totally different as proposed/calculated in CA process. Hence, it is expected that all defect related properties, particularly structural, optical and magnetic can be tailored by MSA.

Objective 2: Origin of polychromatic emission and defect distribution within annealed nanocrystalline ZnO and their effect on magnetic properties and spin-spin interaction.

(a) Optical and magnetic properties

Absorption data in figure 4(a) shows that there is no any effective change in band gap (E_g) after annealing (E_g was estimated from Tauc fit to experimental data points). In absorption data we observed broad band tail region with low energy absorption peak at 2.51 eV and 2.35 eV in pristine and one extra peak at 2.20 eV in annealed sample respectively. Broadband tails were attributed due to stress, whereas absorption peak in visible region were assigned due to V_O, V_O^+ and V_{Zn} respectively. This is because, spatial distribution of defects are inhomogeneous within the sample, hence, they create inhomogeneous local pressure which lead to fluctuations of energy gap, which appear as band tail in absorption curve. Three different excitation energy 3.54 eV (350 nm), 3.10 eV (400 nm) and 2.75 eV (450 nm) were chosen to excite ZnO sample for photoluminescence (PL) measurement. On excitation with photons of energy 3.54 eV all ZnO samples (annealed below 800 ^{0}C) exhibit a excitonic emission in UV region (near band edge emission, NBE) and in visible region (blue, green and yellow) which is associated with intrinsic defect, figure 4(b) and figure 4 (c). PL peaks were identified using Gaussian de-convolution, which is shown as colored dotted lines; their peak position is marked with arrow. It is interesting to note that after annealing at 1000 ^{0}C and 1100 0C peak intensity of NBE decreases and defect related peak increases with red shift of 20-30 meV. This indicates increase of surface defect due to high temperature annealing (T>1000 ^{O}C), figure 4(d). Quenching of NBE and the enhancement of defect related peaks is due to recombination of trapped electron in conduction band with deeply trapped hole at oxygen vacancy and oxidation of surface of grain or both. Increase of ratio of peak intensity of NBE to zinc defect and oxygen defect with annealing temperature indicates that surface defect are solely responsible for both, quenching of NBE and enhancement of defect related

peaks, figure 5(e). The intensity ratio of the NBE to visible emission for spherical grain of radius *R'* and with a surface recombination thickness *t'* is given by $\frac{I_{NBE}}{I_{visible(Zn/V_O)}} = C(\frac{R'^3}{3R't'(R'-t')+t'^3}-1)$,[13], Where C is a constant, which contains oscillator strength and is independent of *R'* and *t'*. It is evident from equation one that intensity ratio will have minimum value at *R'=t'*, which indicate maximum allowed growth, and maximum allowed annealing temperature, for ZnO it is 1100 ^{0}C. Different region for temperature driven growth and surface defect dominance is marked with dotted lines in figure 5(f). Dominance of surface defect occurs near *~t'=R'/7*, hence range of surface recombination thickness can be taken as *R'/7<t'<R'*. Our grain size analysis shows maximum value of *t'= R'/2*. Presence of intrinsic point defects (Zinc interstitial Zn_i, Oxygen vacancy V_O, Zinc vacancy V_{Zn}) controls optical emission in visible range. Whereas, electron or hole trapped at these point defects serve as paramagnetic centers. Direct or indirect exchange interaction between these charged defects governs magnetic properties of un-doped nanocrystalline ZnO. We had observed defect pair of (V_O-Zn_i) and (V_{Zn}-Zn_i) by electron spin resonance (ESR) spectroscopy at low temperature (125K, temperature less than binding energy of bound excitons). Observation of defect pairs reveals that green emission from ZnO consist of some new mechanism. When ZnO sample is excited with photon of energy larger than band gap ($h\nu > E_g$) the green emission is due to transition from V_O to valance band. Whereas, when no band states are involved in absorption e.g. when sample is excited with photon of energy less than band gap ($h\nu < E_g$), then instead of band excitation, internal atomic excitation takes place, which results into singlet excited state. From this singlet state an inter system crossing occurs to the spin and orbital triplet emitting state . The radiative recombination from triplet state of V_O (spin, S=1) to singlet ground state of V_O (spin, S=0) causes green emission. It is like 3P to 1S type recombination where band state of ZnO are not involved. All annealed

sample in temperature range 200-800 ^{0}C including pristine show ferromagnetic behavior, which get saturated at very low magnetic field ~1500 Gauss. Whereas, sample annealed at 1100 ^{0}C reveals diamagnetic nature, figure 5(a).Low saturation and embedded diamagnetic character may be due to defect cluster/ defect pair formation. In order to investigate origin of ferromagnetic nature of undoped ZnO, and transition from ferromagnetic to diamagnetic behavior, we did ESR measurement in temperature range of 125K to 275K on 400, 800 and 1100 ^{0}C annealed sample. Because, 400 ^{0}C annealed sample is rich in defects, 800 ^{0}C annealed sample shows enhanced. Surface properties and 1100 ^{0}C sample shows re-distribution of defects. Figure 5(b), 5(c) and 5(d) show ESR spectra of 400 and 1100 ^{0}C annealed sample respectively. Calculated g value at 1.965, 2.007, and 2.012 shows presence of ionized Zn_i, V_O, and V_{Zn} defects respectively. Lorentzian de-convolution of ESR spectra also reveals formation of ionized defect pair Zn_iV_{Zn} and Zn_iV_O at g= 1.999 and 1.993 respectively. Interestingly, ESR spectra of 800 ^{0}C annealed sample shows only one broad and asymmetric signal at g=1.966, this indicates that Zn_i is located in surface region or at grain boundary. Therefore it is expected that ferromagnetic nature of undoped ZnO is due to presence of multi domains, schematically shown in inset of figure 5(a). Direct exchange interaction between Zn_i and V_{Zn} or defect pairs via conduction electron causes ferromagnetism. This result is further supported by ESR spectra of 1100 ^{0}C annealed sample, where there is no any signature of Zn_i signal, only deep defects and defect pairs were observed. . These deep defects only serve as mediator for enhancing ferromagnetic coupling between shallow donors.

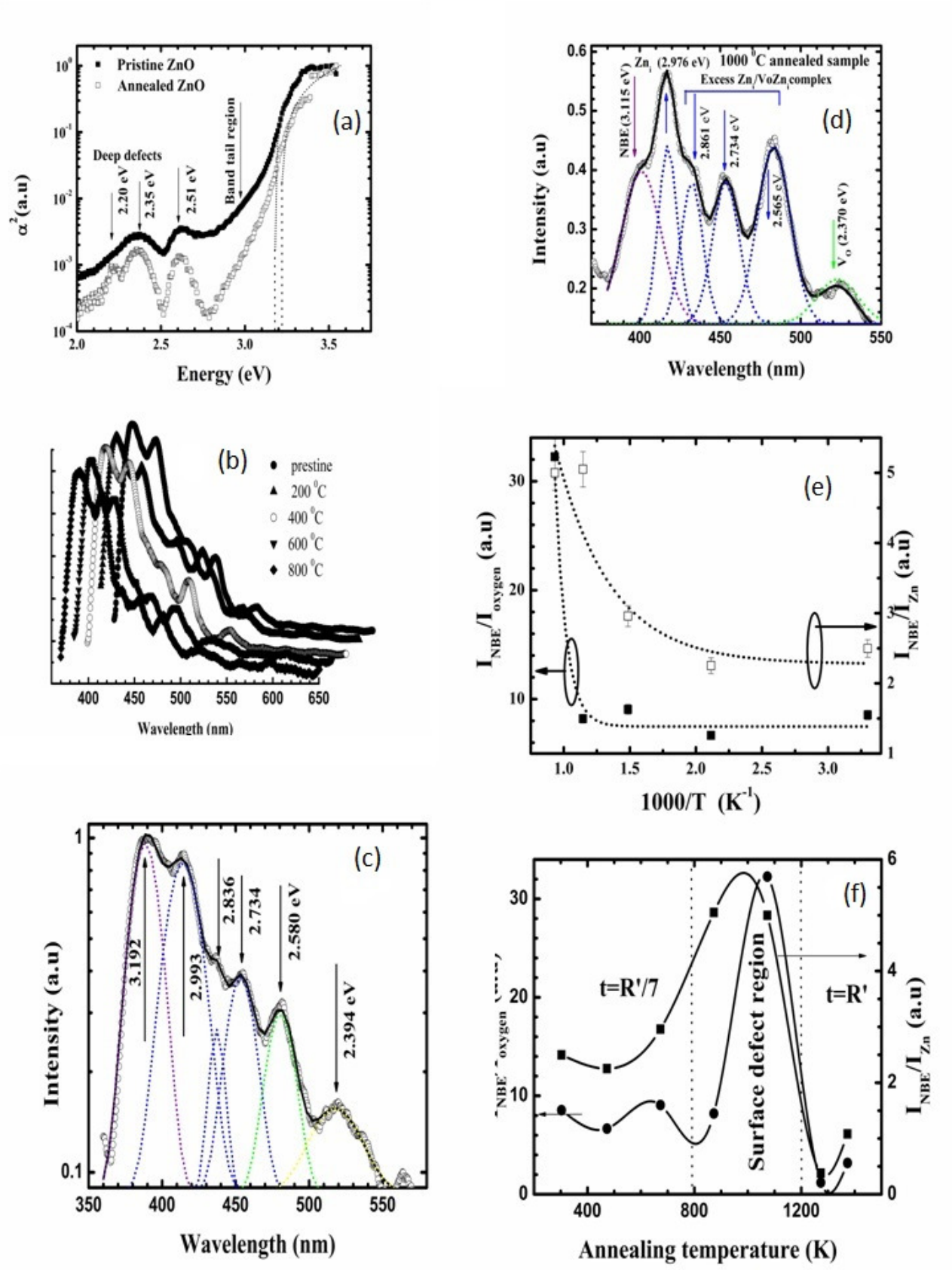

Figure 4: Absorption and optical emission spectra of conventional annealed ZnO.

3: Selectively enhanced different defect in nanocrystalline ZnO: A path to make p-type ZnO without doping by multistep annealing.

To elaborate the photoluminescence properties, the samples were excited from excitation wavelength 300nm (photon energy $h\nu > E_g$) and 400nm (photon energy $h\nu < E_g$) figure 6(a) and 6(b) respectively. The peak at 3.19eV is the band to band transition or near band edge emission (NBE). It doesn't change till 600ºC but a little blue shift in NBE peak at 800°C can be seen from graph, which could be attributed to excess oxygen vacancies. The NBE is quenched at 200°C, 400°C and 600°C and the suddenly gets enhanced at 800ºC together with emission spectra in visible region from 400nm to 575nm which is attributed to intrinsic defect states lying between the valence band and the conduction band. Effect of these intrinsic defects on crystal structure were analyzed using Ramman spectra which reflects optical phonons at Γ point of the first Brillouin zone. The irreducible representation at Γ point is: $\Gamma_{opt} = A_1 + E_1 + 2E_2 + 2B_1$. Where, both polar modes A_1 and E_1 and non-polar mode E_2 is Raman active. Nonpolar phonon modes with symmetry E_2 have two frequencies: E_2 high associated with oxygen atoms and E_2 low associated with Zn sub lattice [14]. E_2^{high} phonon mode is characteristics Raman mode of wurtzite ZnO, figure 6(c). The changes in line shape/broadening and a little shift to higher and lower wave number depicts the compressive and tensile strain in the sample due to intrinsic defects in the sample. The figure 6(d) shows that the E_2^{high} mode of 600°C is fitted with one Lorentzian peak centred at 445.86cm^{-1}. Whereas in 800 ^{0}C MSA sample the splitting of E_2^{high} is visible and was fitted with it in two Lorentzian peaks centered at 423.15cm^{-1} and 434.57cm^{-1} it reveals that the two different peaks are coming separately from vibrations of the oxygen in the wurtzite lattice, figure 6(e). The change in the oxygen composition or structure around it can be seen indirectly by broadening of asymmetrical Raman mode E_2^{high} till 600°C and indifferently splitting in two different peaks at 800°C. The proposal of enhanced V_o from photoluminescence was then substantiated from the Raman mode E_1(LO), which is directly associated with the V_o.

The excessively enhanced green emission at 800°C and broadly enhanced peak at 576.55cm^{-1} (E_1(LO)) confirmed the existence of excessively enhanced V_o [15].

M-H curve of all MSA samples has been plotted after removing the diamagnetic background. It is observed that the sample annealed at 800°C is purely diamagnetic in nature. Whereas, samples annealed at 200°C, 400°C and 600°C shows ferromagnetic nature. The highest value of Ferromagnetic moment (M_s= 0.00136emu\gm) is observed for samples sintered at 400˚C.

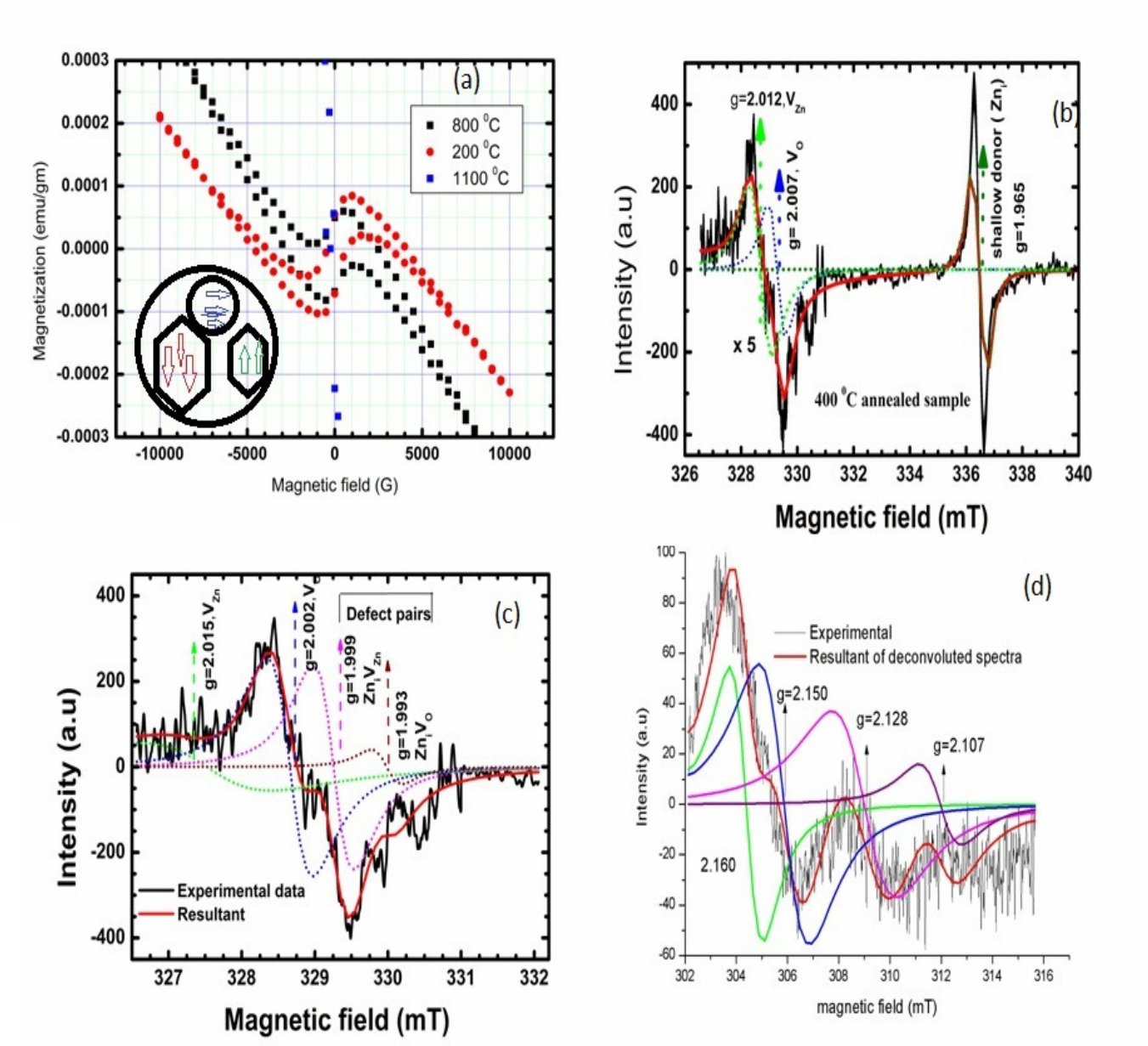

Figure 5: ESR spectra of 400, 800 and 1100 ^{0}C annealed sample at 125K.

This value of the magnetic moment is in good agreement with the recently published papers [16]. The room temperature ferromagnetism in sintered ZnO nanoparticles is an expected result at 200°C, 400°C and 600°C but a transition from ferromagnetism to diamagnetism is quite a new. Huge efforts have been put into the investigation of the mechanism of room temperature ferromagnetism (RTFM) in ZnO even when it contained no transition-metal adulteration [17] The explanations of room temperature ferromagnetism vary from authors to authors as some of them believe it to be lattice defects like zinc interstitial (Zn_i), zinc vacancies (V_{Zn}), oxygen interstitials (O_i), oxygen vacancies (V_o), antisite Zn/O and complexes (V_o-Zn_i), defect clusters, and non stoichiometric porous region at grain boundaries [18].

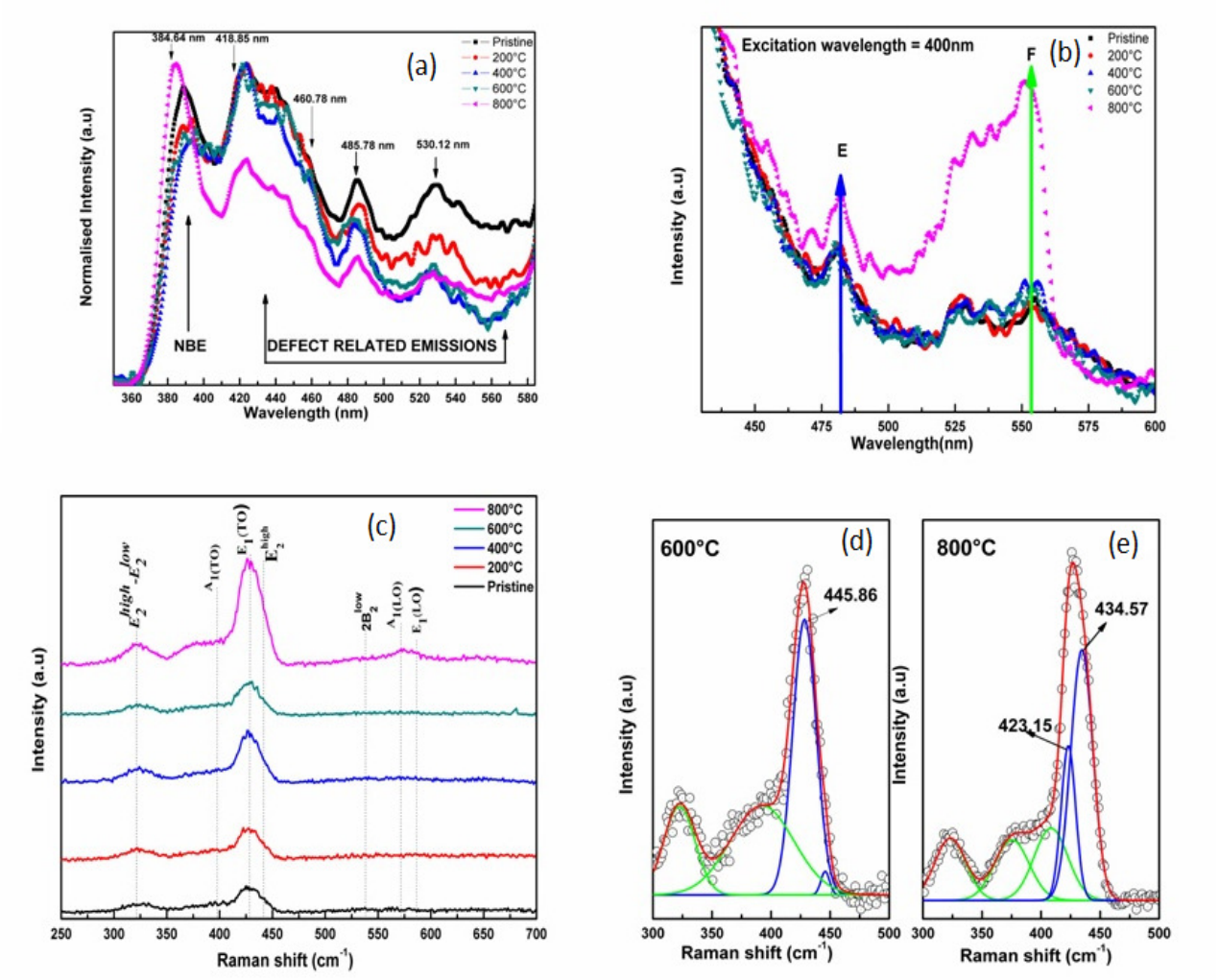

Figure 6. Photoluminescence and Ramman spectra of the MSA samples

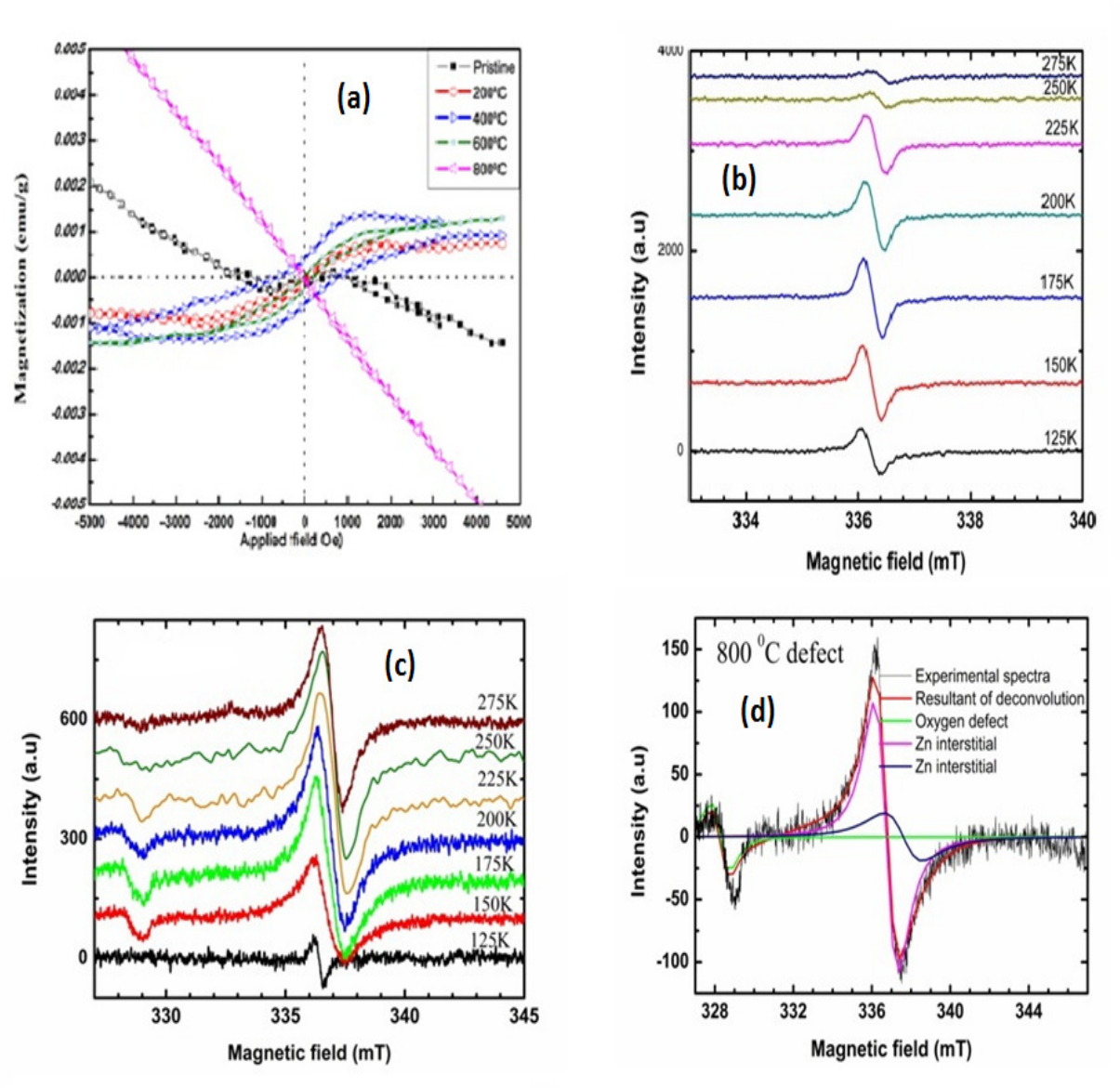

Figure 7: M-H curve (a) and ESR spectra of multi step annealed sample at 400 ^{0}C (b) and 800 ^{0}C (c) respectively, de-convoluted spectra of 800 ^{0}C MSA sample at 125K.

In order to investigate the origin of ferromagnetism in un-doped MSA sample and temperature induced transition from ferromagnetism to diamagnetism at 800 ^{0}C as compared to conventionally annealed samples, temperature dependent ESR were performed on 400 ^{0}C and 800 ^{0}C MSA sample. ESR spectra of these MSA samples are shown in figure 7 (b) and 7(c) respectively. Whereas, figure 7(d), shows de-convoluted ESR spectra at 125K. 400 ^{0}C MSA show only Zn_i line which as broad and asymmetric as compared to CA samples. This indicates formation of surface polaritons, surfaces Zn_i and enlarge spin lattice interaction,

whereas 800 ^{0}C MSA sample shows Zn_i as well as V_o. Although, there is no any signature of defect pairs. Hence room temperature ferromagnetism in MSA sample is due to surface defects only. This is cross verified from grain growth and PL spectra.

4: Development of CoO and NiO doped ZnO nanoparticles: A promising dilute magnetic semiconductor material for spin aligner.

From the physics point of view, study of DMS in solid state is interesting and very complex too, because local state of magnetic ions placed at different site of crystal shows different spins configuration. For example Co^{+2} at octahedral site and tetrahedral site have low spin configuration and high spin configuration respectively as shown in figure 8(a) . Therefore, mutual interaction of these spins cause different atomic radii at different lattice site. In ZnO wutrzite structure, Zn and O both occupy tetrahedral geometry. Hence Co replacing Zn iso-electronically have different property and isolated Co or cluster of CoO e.g Co-Co dimer interaction (direct or via defect) will have different effect on Zeeman splitting and exchange interaction . Therefore , ESR spectra of CoO doped ZnO contains an additional term of hyperfine interaction due to nuclear spin and structural factor { axial symmetric part (D) and assymetrical parameter (E)}. An example of hyperfine nuclear transition in Co and simulated spectra of Co-Co dimmer is shown in figure 8(b) and 8(c) .

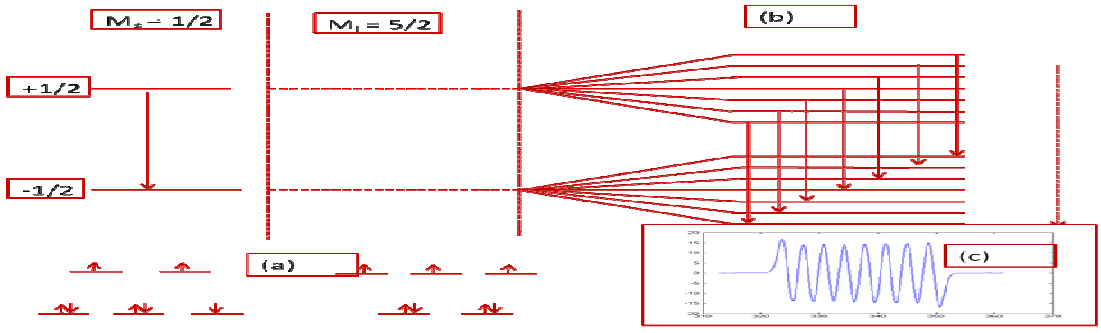

Figure 8: Schematic of nuclear fine structure and splitting of d- orbital's in crystal fields.

We had performed ESR of CoO, and NiO doped ZnO in wt % of 1,2,4,6,8 ,10 and 0.5,1,2.5,3 respectively, in temperature range of 5K to 100K in X band.Co^{+2} has nuclear spin 5/2 hence we expect 7 ESR lines in nuclear hyperfine structure, which is shown in figure 9(a). Only 1 % CoO doped ZnO reveals hyperfine structure. Rest of the sample does not show any signature of hyperfine interaction. Further, powder sample is polycrystalline in nature hence $g_{\parallel}$ (when applied magnetic field B is parallel to c-axis)at 2.24 and $g^{\perp}$ (when applied magnetic field B is perpendicular to c-axis) at 4.28 were observed simultaneously. Interestingly nuclear hyperfine structure was observed in parallel configuration only. Surprisingly, with increase of CoO % doping we did not observe any hyperfine splitting as shown in figure 9(b), this is due increase of asymmetry parameter E and decrease of axial symmetry parameter D. Although, ESR line width increases linearly with increase of doping faction. This reveals strong spin-spin and spin lattice interaction. Change in structural parameter was characterized by XRD and Ramman spectra as shown in figure 10 and 11 respectively. From XRD measurement we observed that lattice constant a,c and unit cell volume first decreases then increases for >2% doping. But c/a ratio decreases linearly with increasing doping %. This is because for 1 % doped sample annealing causes diffusion of Co along crystal c direction and it suppress further diffusion along c axis. This change can be attributed due to small difference in the ionic radii between the Zn^{+2} (0.60 A^0) and the Co^{+2} in high spin configuration (0.58 A^0). It is important to notice that although a, c and V increases with increasing % doping but this change is very nominal e.g. of the order of difference of ionic radii of Co^{+2} and Zn^{+2}. The minimal change exhibited in a,c and V proves that Co ions are not at the octahedral interstices of the wurtzite structure as this would lead to a significant increase in these quantities because octahedral divalent Co has radius between

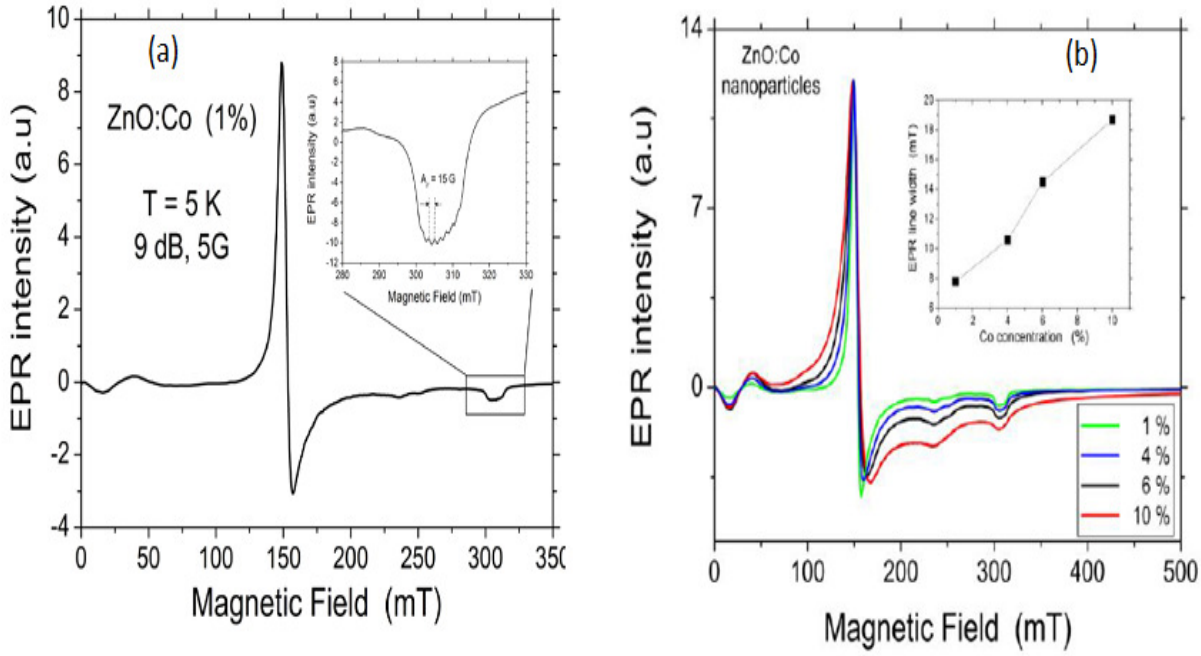

Figure 9: Low temperature ESR spectra of 1% Co doped sample. Inset shows hyperfine structure and increase of EPR line width with doping %.

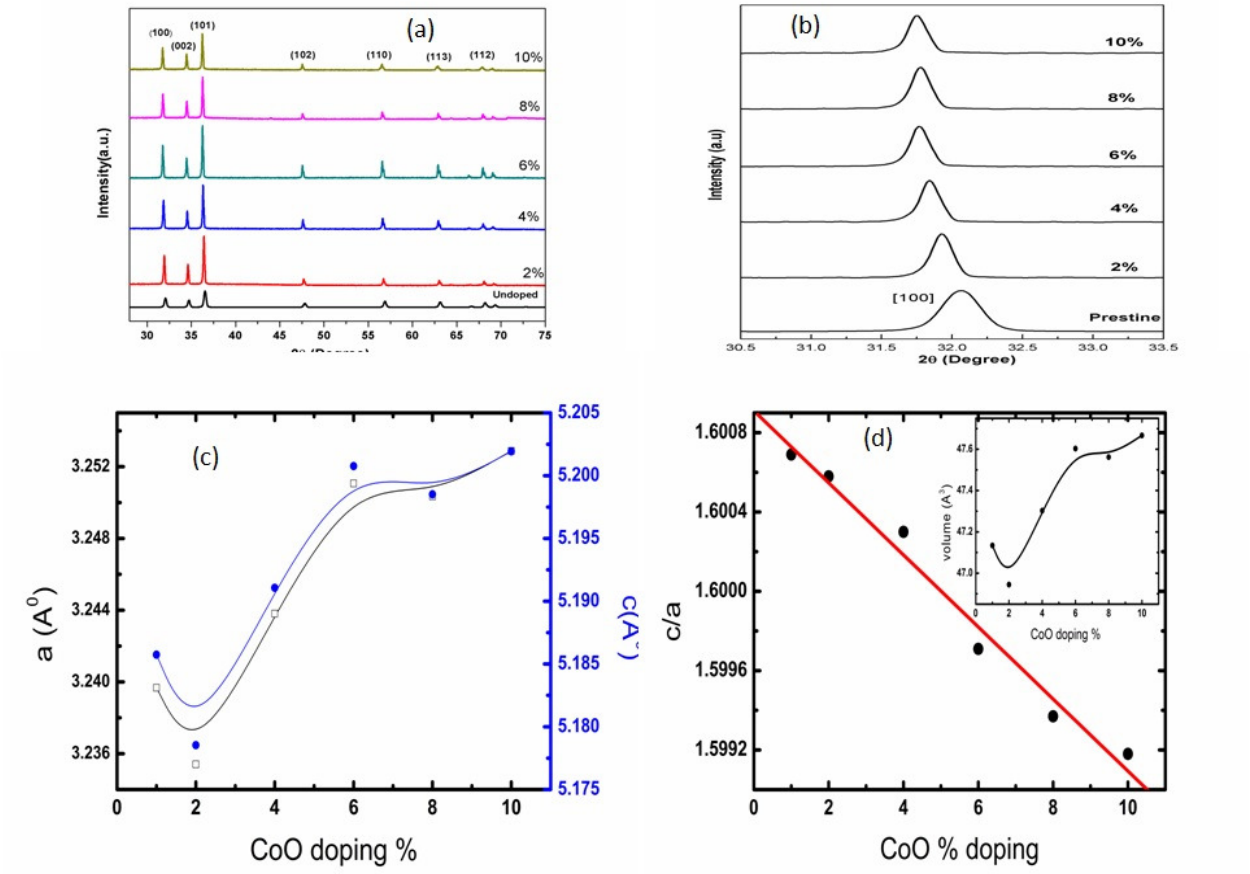

Figure 10: Evolution of lattice parameter of ZnO on CoO doping

0.65 A^0 (low spin) and 0.75 A^0 (high spin).Further considering (i) the splitting of d-orbital in tetrahedral field is smaller than octahedral field (Δ_{tet}=4/9 Δ_{oct}), (ii) crystal field splitting of wurtzite ZnO~ 31 meV is larger than Δ_{tet} and (iii) spin-orbit interaction in ZnO (~ -19 eV) same as spin-orbit coupling of Co ions, we expect hyperfine splitting in all samples . Unfortunately, hyperfine splitting was seen only in one sample (1% CoO doped sample). Whereas, Zero field resonance was present in all sample. Ramman spectroscopy were performed to investigate the local structure around magnetic atom in terms of their distribution, cluster formation and segregation of phase,. This is because XRD measurement is not sensitive enough to detect clusters because of strong absorptive nature of metal cluster in X-rays regions. Figure 11, shows the Ramman spectra of CoO doped ZnO, figure 11(a) and (b). Figure 11 (c) and (d) shows enhanced Ramman peak for 10% CoO doped sample. A comparatively weak and broad Ramman band at 484 cm^{-1} is due to surface phonons. With the doping two interesting facts were noticed (i) enhancement and broadening of phonon modes, and (ii) sharpening of phonon bands after 6% CoO doping. The broadening of phonon mode reflects the deterioration of the host lattice by the distortion of local atomic arrangement around magnetic impurity and sharpening of peaks resembles the phonon modes of Co_2O_4 e.g. CoO clusters which were not detected by XRD measurement. Therefore, origin of intrinsic ferromagnetic nature in ZnO based DMS is questioned by Ramman and easily get answered by spin measurement because if cluster formation takes place Co-Co dimmer is more likely to occurs but we did not observed any signature of dimmer in ESR. This shows negligible amount of Co_2O_4 phase. Influence of CoO doping on ferromagnetic nature was then studied in non conventional method other than VSM measurement. In this non conventional method ESR signals were reproduced in rising and falling magnetic field, figure 12. This shows shift of ESR signal by 12G, which indicate small amount of metallic Co, which slightly

shift the resonance line when magnetized. This also suggests that geometrical configuration (orientation of applied magnetic field with respect to crystal direction) also affect magnetic properties. For different CoO doping % ESR signal was normalized. Normalization reveals that ESR lines get broader with increase of doping due to dipolar broadening or spin-spin interaction. Our new finding is magnetic states/ fine structure around magnetic ions. There were at least 10 ESR lines around Co ions, there intensity increases with increasing microwave power, figure 13. Microscopic origin of these lines is not clear yet. However, we suspect formation of new magnetic phase by interaction of Co, oxygen and Co. In order to see Co-O-Co like structure, room temperature FTIR was also performed, but we did not get it signature. We hope that low temperature Ramman and low temperature FTIR may give some signature of Co-O-Co interaction or bond formation. NiO doped ZnO is not a good candidate for DMS and spintronic devices because Ni ion in tetrahedral co-ordination has zero spin in ground state, henxe it will not give any ferromagnetic and ESR signal. However, its excited state (just above the ground state) is two fold degenrate and has pseudo spin ½ and may give some signal when get populated . Figure 16 shows ESR spectra of 0.5 % NiO doped ZnO. In this figure, we recognize the Co2+ powder signal by its form and its position (150 mT). The big structure around 340 mT is recognized as Mn2+ powder signal because of its global position. Another point allowing identification is that Co2+ relax very quickly because of its big spin-lattice coupling, so that the EPR intensity is expected to decrease rapidly with temperature, whereas, on the contrary, Mn2+ ions relaxes slowly, and have a weak temperature dependence of their EPR lines. It is important to mention that host material was 99.99 % pure and CoO and NiO were 99.5 and 99 % pure (as claimed by Sigma-aldrich), even though we observe strong magnetic and ESR signal from impurity.

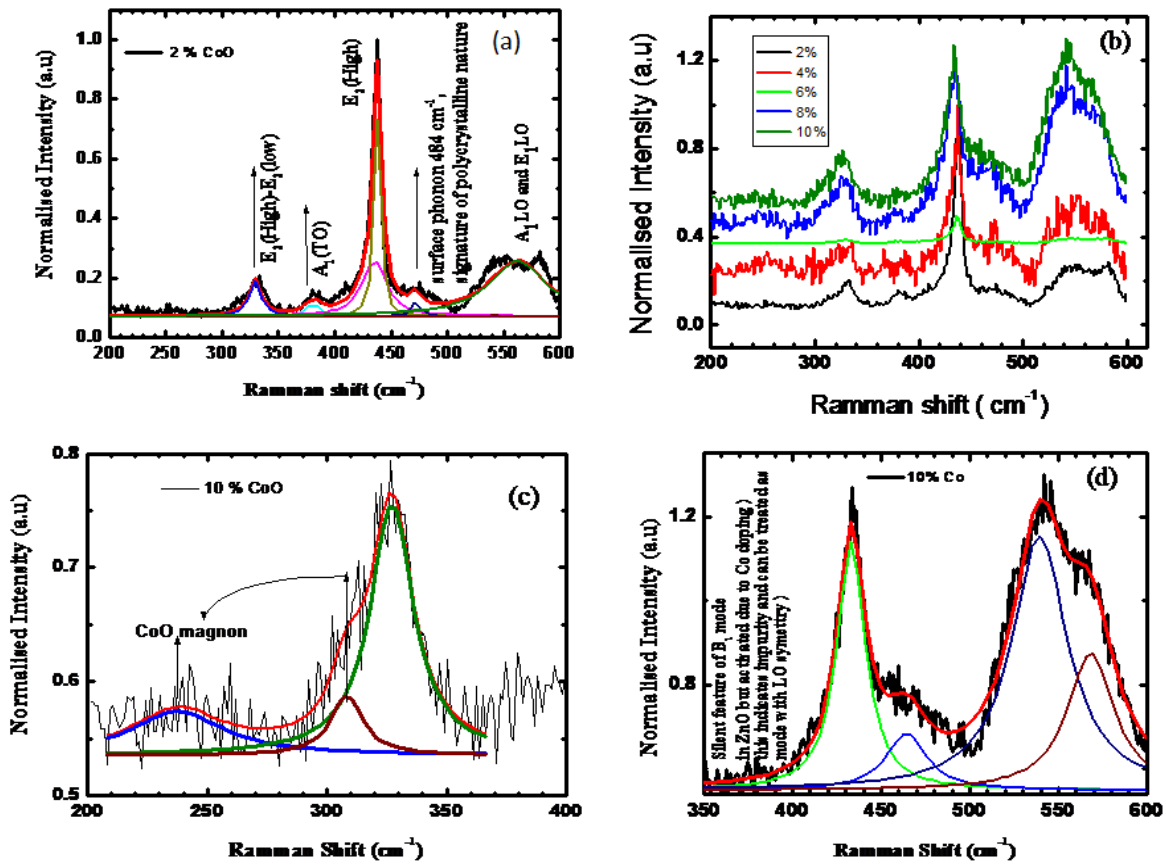

Figure 11: Ramman Spectra of doped as well as undoped samples.

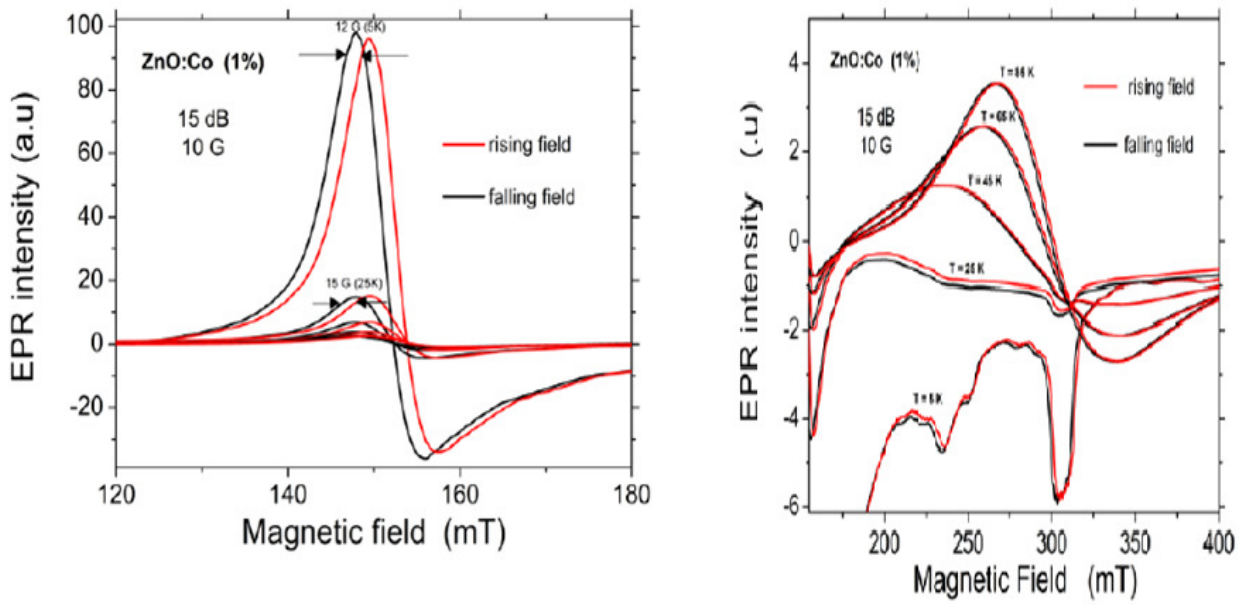

Figure 12: ESR signal in rising and falling magnetic fields

Hence, powder samples grown by wet chemical method or sol-gel techniques and thin film made by spin coating will not be good material for making spin-tronic devices. Only thin films made by atomic layer deposition (ALD) method or pulsed laser deposition (PLD) methods at high substrate temperature can be suitable method for making spin based devices. In future, we would like to make this device and test it by emission of polarized light by electroluminescence measurement. It will also be interesting to study spin relaxation and domain mapping in DMS.

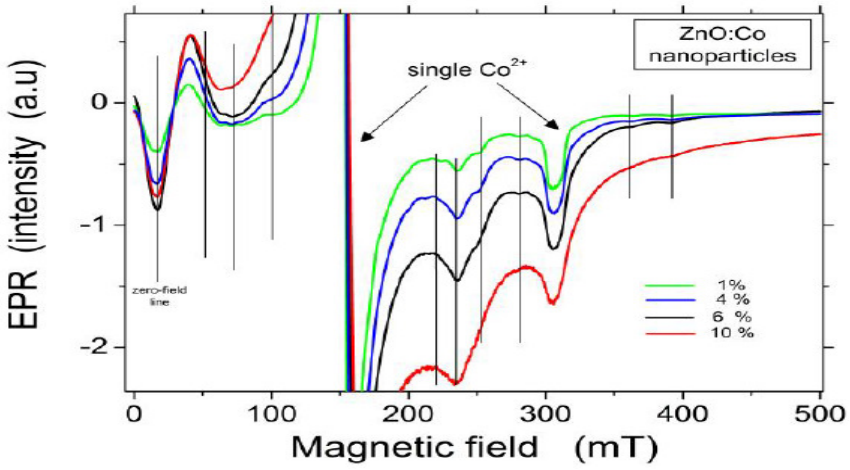

Figure 13: New magnetic states around Co ions in ZnO

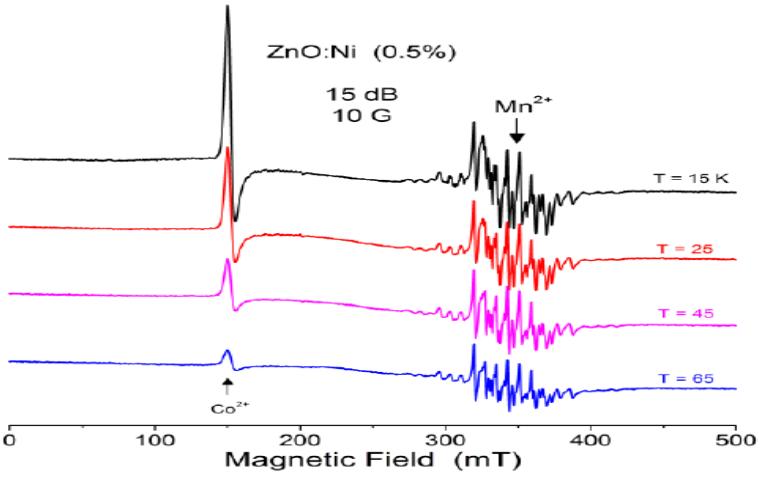

Figure 14: ESR Spectra of NiO doped sample at different temperature.

References:

[1] S.J. Pearton et.al , " ZnO Spintronics and nanowire Devices", Journal of Electronic materials, Vol 35, 862 (2005).

[2] Stefan T. Ochsenbein, Yong Feng, Kelly M. Whitaker, Ekaterina Badaeva, William K.Liu,Xiaosong Li and Daniel R. Gamelin, " Charge-controlled magnetism in colloidal doped semiconductor nanocrystals", Nature nanotechnology,Vol 4 ,681 (2009).

[3] R.Fiederling, M.Keim,G.Reuscher,W.Ossau, G.Schmidt, A. Waag and L.W.Molenkamp, " Injection and detection of a spin-polarized current in a light-emitting diode" ,Nature , Vol402, 787 (1999).

[4] Y.Ohno,D.K.Young,B.Beschoten,F.Matsukura,H.Ohno and D.D. Awschalam " Electrical spin injection in ferromagnetic semiconductor heterostructure", Nature, Vol402, 790 (1999).

[4] Kelly M. Whiyaker, Maxim Raskin et-al." Spin-on Spintronics: Ultrafast Electron Spin Dynamics and ZnO and $Zn_{1-x}Co_xO$ Sol-Gel Films" , Nano Letters , Vol 11,3355 (2011).

[5] T. J. Castro, P. A. M. Rodrigues, A. C. Oliveira, F. Nakagomi, J. Mantilla, J. A. H. Coaquira, A. Franco Junior, H. V. S. Pessoni, P. C. Morais, and S. W. da Silva " Optical and magnetic properties of Co doped ZnO nanoparticles and the onset of ferromagnetic ordering" J.Appl.Phys, Vol 121, 013904 (2017).

[6] Paul I.Archer, Steven A. Santangelo, and Daniel R. Gamelin, " Direct Observation of sp-d Exchange Interactions in Colloidal Mn^{2+}-and Co^{2+} Doped CdSe Quantum Dots", Nano Letters, Vol 7, 1037 (2007).

[6] A Savoyant, H Alnoor, S Bertaina, O Nur and M Willander "EPR Investigation of pure and Co-doped ZnO oriented nanotstructure", Nanotechnolgy", Vol 28, 035705 (2017).

[7] D.C Reynolds, D.C. Look and B.Jogoi "Polariton and free exciton like photoluminescence in ZnO", Appl.Phys.Lett, Vol 79, 3794 (2001).

[8] G. W. Tomilns, and J. L. Routbort, Oxygen Diffusion in Single-Crystal Zinc Oxide, J. Am.Ceram.Soc , Vol 81 869 (1998).

[9] D.J Binks, PhD thesis , University of Surrey, 1999.

[10] V. J. Lee, G. Parravano, Sintering reactions of zinc oxide, J. Appl. Phys, Vol 30 1735 (1959).

[11] Neha Kondal and Sanjiv Kumar Tiwari " Origin of polychromatic emission and defect distribution within annealed ZnO nanoparticles" Materials Research Bulletin, Vol 88,156 (2017).

[12] Xinyu Zhang et.al " Effect of aspect ratio and surface defects on the photocatalytic activity of ZnO nanorods" Scientific Reports, vol 4, 4596 (2014).

[13] I. Shalish, H. Temkin, V. Narayanamurti, Size-dependent surface luminescence in ZnO nanowires, Phys.Rev B, Vol 69 245401 (2004).

[14] Khan A. Alim, V.A. Fonoberov, M. Shamsa, A.A. Balandin, Micro-Raman investigation of optical phonons in ZnO nanocrystals, J. Appl. Phys. Vol 97, 124313 (2005).

[15] Neha Kondal and Sanjiv Kumar Tiwari "Selectively enhanced oxygen vacancies in undoped polycrystalline ZnO as a consequence of Multi-Step Sintering" Ceramic International, Vol 43,10347 (2017).

[16] T. Dietl, H. Ohno, F. Matsukura, J. Cibert, and D. Ferrand, "Zener model description of ferromagnetism in zinc-blende magnetic semiconductors" , Science, Vol 287 1019 (2000).

[17]_A. Savoyant, F. Giovannelli, F. Delorme, and A. Stepanov " EPR characterization of Co-doped ZnO microwires and distant spin-pair coupling" , Semicond. Sci. Technol. Vol 30 075004, (2015).

[18] Qian Wang et.al "Vacancy Induced magnetism in ZnO thin film and nanowires", Phys. Rev B, Vol 77, 205411 (2008).